RSC Advances

ROYAL SOCIETY OF CHEMISTRY

www.rsc.org/advances

A *Meta*-Molecular Tailoring Strategy Towards Efficient Violet-Blue Organic Electroluminescent Material

Wen-Cheng Chen,[a,b] Guang-Fu Wu,[a] Yi Yuan,[a,b] Huai-Xin Wei,[b] Fu-Lung Wong,[b] Qing-Xiao Tong*[a] and Chun-Sing Lee*[b]

[a] Department of Chemistry, Shantou University, 243 University Road, Shantou, Guangdong, 515063, P.R. China.
E-mail: qxtong@stu.edu.cn

[b] Center of Super-Diamond and Advanced Films (COSDAF) and Department of Physics and Materials Science, City University of Hong Kong, Tat Chee Avenue, Kowloon, Hong Kong SAR, P. R. China.
E-mail: apcslee@cityu.edu.hk

Abstract

In this paper, an efficient violet-blue emitter 4,4"-bis(1-(4-(*tert*-butyl)phenyl)-1*H*-phenanthro [9,10-*d*]imidazol-2-yl)-1,1':3',1"-terphenyl (***m*-BBTPI**) was designed and synthesized by linking two phenanthroimidazole units via the *meta* position of a freely rotatable phenyl bridge. The present design provides a suitable level of conjugation between the two phenanthroimidazole units such that fluorescence is strengthened over the single unit while a violet-blue emission can be maintained by limiting the amount of redshift. The new emitter ***m*-BBTPI** is also found to have good thermal stability, strong violet-blue emission and bipolar charge transporting properties. An electroluminescent device using ***m*-BBTPI** as a non-doped emission layer shows a low turn-on voltage (3.2 V), good colour purity (0.16, 0.06) as well as high current and power efficiencies (1.99 cd A^{-1}, 1.81 lm W^{-1}). These performance parameters are comparable to the state-of-the-art non-doped violet-blue OLEDs.

Keywords: phenanthroimidazole, *meta*-tailoring, violet-blue emission, organic electroluminescence.

1. Introduction

Violet-blue light-emitting materials are used in multifarious applications, such as phototherapy,[1] photocopying,[2] sterilization,[3] drinking-water purification *etc*.[4] Especially, high-energy violet-blue emitters can not only serve as energy donors to excite lower-energy dopants for achieving white light emission,[5] but also play a key role in reducing power consumption in full-colour displays.[6] Currently, the most conventional approach for getting violet-blue emission is to convert the 254-nm-emission of low-pressure Hg discharge to the desired colours by using $Sr_2P_2O_7$:Eu^{2+} phosphors.[7] However, mercury is a strong neurotoxin and its use is considered to be not eco-friendly.[8] Organic light-emitting devices (OLEDs) could be a potential alternative to generate violet-blue emission. On one hand, by using suitable emitters, OLEDs can directly generate violet-blue emission without using any additional photo-converter. On other hand, it can serve as Hg-free and relatively eco-friendly light sources for the green environment. However, so far, materials for violet-blue OLEDs exhibiting high efficiency and meeting the requirements of standard colour purity (0.15, 0.06) are rarely reported.[6b,9] For an emitter to emit in violet-blue, a wide energy gap is a prerequisite. However, the wide energy gap typically lowers the efficiency of carrier injection and transportation, leading to higher operation voltage and shorter operation lifetime.[10,11]

Furthermore, the wide energy gap is often achieved by confining the extent of π-conjugation and this would typically reduce the fluorescent quantum yield.[12]

In the exploration for high-performance violet-blue emitters, phenanthroimidazole (PI) derivatives have drawn much attention due to their facile synthesis,[6b,9d,9e,13] high fluorescent quantum yields,[9d,13a,13c,13e] appropriate π-conjugation for violet-blue emissions[6b,9d,9e,13a,13d,13e] and good thermal stabilities.[6b,9d,9e,13] Additional, PI compounds also serve as efficient hosts for phosphors due to their relatively high triplet energy level.[13h-m] Moreover, the different electronic properties of the two nitrogen atoms[14] in PI endow them with both hole[13d] and electron transporting capabilities.[13a-c] For example, Ma's group has successfully developed a high-efficiency bipolar blue emitter by linking two 1,2-diphenyl-1*H*-phenanthro[9,10-*d*]imidazole (PPI) units.[15] However, while the use of two emitting units does substantially enhance the fluorescence and device efficiencies, the extended molecular conjugation can lead to considerable emissive redshifts.

In order to obtain efficient violet-blue emitters, it has been suggested that by changing the molecular linkage from *para*- to *ortho*- or *meta*-modes, the extent of conjugation could be well confined.[10a] Nevertheless, there are few works using this strategy to achieve violet-blue emission and high device performance simultaneously. For instance, Huang *et al*. reported a series of 4,4'-bis(1,2,2-triphenylvinyl)biphenyl (BTPE) derivatives via *ortho*- or *meta*-linkages, achieving deeper blue electroluminescence (EL). However, comparing to the *para*-counterpart compound BTPE, the *ortho*/*meta*-linked compounds failed to maintain the high device performances, with maximum external quantum efficiency (EQE) ranging from only 1.4 to 1.9%. Recently, taking advantages of the PI derivatives and the non-*para* linkage, Wang *et al*. designed and synthesized two dimeric PI compounds, *L*-BPPI and *Z*-BPPI, so as to blueshift the sky-blue emission of 4,4'-bis(1-phenyl-phenanthro[9,10-*d*]imidazol-2-yl)biphenyl (BPPI).[16] However, the colour purities and efficiencies of the *L*-BPPI- and *Z*-BPPI-based devices still have room for improvement. Suitable molecular tailoring for the emitters and device structure are needed to fundamentally boost the device performances.

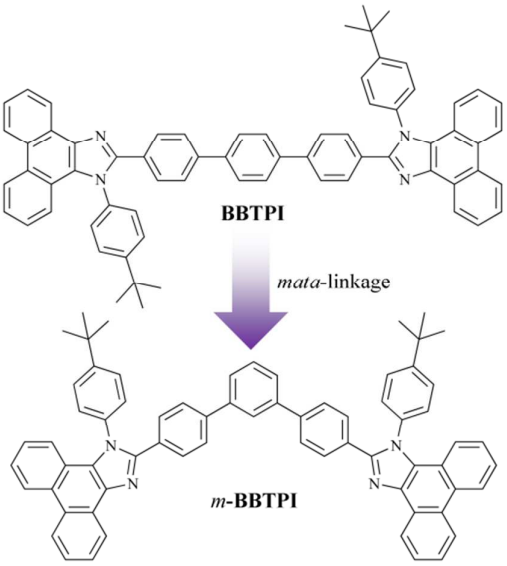

Scheme 1 Molecular structure and design strategy of ***m*-BBTPI**.

In this work, a blue emitter 4,4''-bis(1-(4-(*t*-butyl)phenyl)-1*H*-phenanthro[9,10-*d*]imidazol-2-yl)-1,1':4',1''-terphenyl (**BBTPI**)[13e] is used as a prototype for designing the present violet blue emitter 4,4''-bis(1-(4-(*tert*-butyl)phenyl)-1*H*-phenanthro[9,10-*d*]imidazol-2-yl)-1,1':3',1''-terphenyl (***m*-BBTPI**, Scheme 1). Here, we joint two 1-(4-(*tert*-butyl)phenyl)-2-phenyl-1*H*-phenanthro[9,10-*d*]imidazole (TPI) units via a phenyl ring at its *meta*-position. In this design the freely rotatable benzene ring in the molecular center plays a key role in confining π-conjugation due to its tetrahedral electronic conformation.[9c] It is found that this strategy successfully leads to efficient violet-blue emission and also maintains the bipolar transporting properties of the PI unit. On the other hand, the *p*-(*tert*-butyl)phenyl group in each PI core not only provides convenience for the facile synthesis (improve solubility in common solvents), but also serves as an intermolecular-distance controller against aggregation-induced redshifts in solid state. By using ***m*-BBTPI** as a non-doped emitter, we obtained a high-performance (1.99 cd A^{-1}) violet-blue OLED (colour purity: (0.16, 0.06)) based on ***m*-BBTPI**, which is comparable to the reported high-efficiency OLEDs in similar colour gamut.

2. Experimental

2.1 Synthesis

All raw materials and solvents were used directly as received from commercial suppliers without further treatments. Synthesis routes of the new compound are depicted in Scheme S1 in the Supplementary Information.

2.2 Characterization

Absorption and photoluminescence spectra of the new compounds were determined with a Perkin-Elmer Lambda 2S UV-Vis spectrophotometer and a Perkin-Elmer LS50B Luminescence spectrophotometer respectively. ^{1}H NMR was recorded with a Varian Gemin-400 spectrometer. Mass spectra were performed with a PE SCIEX API-MS spectrometer. Elemental analysis (C, H, N) was measured using a Vario EL III CHNS elemental analyzer. Ionization potential (IP) of the material was measured on an ITO substrate in a thin-film state via ultraviolet photoelectron spectroscopy (UPS) in a VG ESCALAB 220i-XL surface analysis system, while electron affinity (EA) was estimated via subtracting from IP with optical band gap. Thermal gravity analysis (TGA) and differential scanning calorimetry (DSC) measurements were recorded with a TA Instrument TGAQ50 and a TA Instrument DSC2910 respectively. Frontier orbital distributions and molecular geometries were calculated through density functional theory with Gaussian 09 program at B3LPY/6-31G(d) level.

2.3 Device Fabrication and Measurement

Pre-patterned indium tin oxide (ITO) glass substrates with a sheet resistance of 15 Ω $square^{-1}$ were cleaned with isopropyl alcohol and Decon 90 solution, then rinsed in deionized water and dried in an oven. After a 15min UV-ozone treatment, the ITO substrates were immediately transferred into a deposition chamber with a base pressure of 5×10^{-7} torr for

organic and cathode depositions. Organic materials were deposited via thermal deposition at a rate of 1 Å s^{-1}, while the cathodes were completed via deposition of LiF (0.1-0.2 Å s^{-1}) and Al (5-6 Å s^{-1}) successively. Electroluminescent spectra and the corresponding Commission Internationale de l'Enclairage (CIE) coordinates were measured with a Spectrascan PR650 photometer. Current-voltage-luminance (*J-V-L*) characteristics were recorded with a Keithley 2400 Sourcemeter under ambient atmosphere without device encapsulation.

3. Results and Discussion

3.1 Synthesis and characterization

Synthetic routes for ***m*-BBTPI** are shown in Scheme S1 in the Supplementary Information. Two steps are involved in the synthesis of the new compound. First, [1,1':3',1"-terphenyl]-4,4"-dicarbaldehyde (***m*-BBCHO**) was synthesized by reaction of 1,3-dibromobenzene and 4-formylphenylboronic acid via a Suzuki-coupling reaction in a mild condition.[17] Second, a "one-pot" reaction[13] was adopted to introduce the PI moieties to construct ***m*-BBTPI**. In this facile two-step process, all the raw chemicals are commercially available and used directly without further purification, and the products were isolated with considerable yields (see Supplementary Information). The molecular structure was determined by ^{1}H NMR, mass spectrometry and elemental analysis.

3.2 Thermal Property

Thermal property of ***m*-BBTPI** was investigated by TGA and DSC measurements under a N_2 atmosphere. Key parameters are listed in Table 1. Generally, materials with high thermal properties can play a key role in combating joule heat, which is often generated during device operation deriving from current injection. Additionally, thermally stable materials are in favour of the process of vacuum deposition. Therefore, OLED materials should be equiped with enough high thermal stabilities. The bulky and rigid structure of ***m*-BBTPI** is beneficial to the thermal stability, as supported by its high decomposition temperature of 512 °C (T_d, 5% weight loss, Fig. 1a). DSC measurements were performed from 50 to 420 °C. During the first heating process, ***m*-BBTPI** only shows an endothermic peak at its melting point (T_m, 360 °C). After heating again, a glass-transition state appears at 190 °C (T_g). Comparing to its *para*-counterpart **BBTPI** (Table 1),[13e] ***m*-BBTPI** exhibits a higher T_d and a comparative T_g, which should be attributed its more bulky and asymmetric molecular configuration. Such a good thermal stability is high enough for general device fabrication and operation.

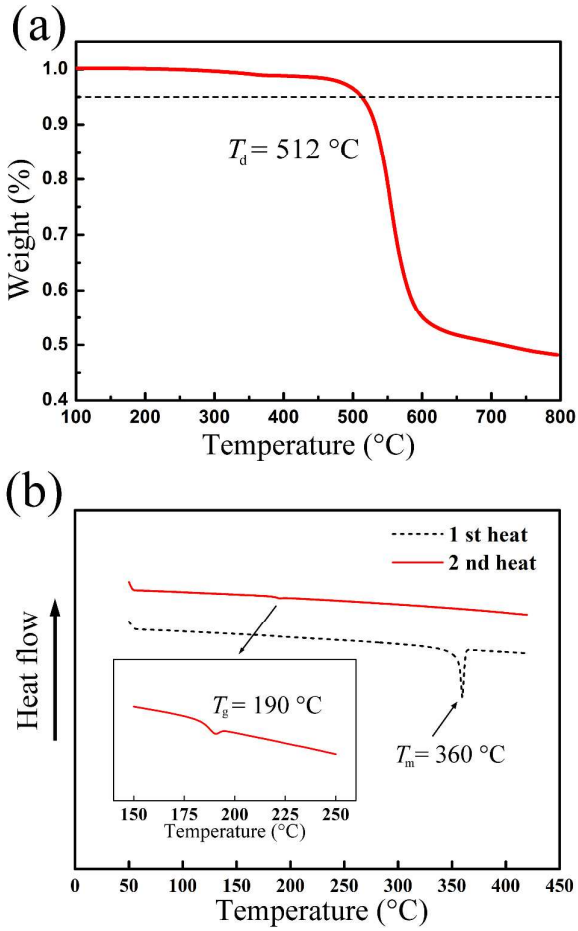

Fig. 1 (a) TGA and (b) DSC measurements of ***m*-BBTPI**.

3.2 Photophysical properties

Fig. 2 presents the absorption and photoluminescence (PL) spectra of ***m*-BBTPI** and **BBTPI** in dilute CH_2Cl_2 solution (10^{-5} mol L^{-1}) and as thin solid film on a quartz plate. Key optical parameters are listed in Table 1. Both of the bisphenanthroimidazole derivatives show analogous photophysical properties. The absorption spectrum in CH_2Cl_2 exhibits a narrow band peaked at ~260 nm with high absorption intensity, which is attributed to the π-π* transition of benzene.[13b] On other hand, a wide band with maxima at ~330 nm are originated from π-π* transition of the PI group.[9d] The new compound ***m*-BBTPI** gives a violet-blue emission peaked at 406 nm in solution shows an evident blueshift in comparison with that of **BBTPI** (λ_{em} = 427 nm). The PL results are consistent with our design idea for violet-blue emitters. Electron delocalization in ***m*-BBTPI** is effectively confined via the *meta*-linkage strategy. Noticeably, the PL spectrum of the ***m*-BBTPI**'s thin film still locates at violet-blue region, and its profile is similar to that of the dilute solution, with only ~20 nm redshift. This suggests that there is little aggregation-induced redshifts via π-π stacking in ***m*-BBTPI** solid. We find that the photoluminescent efficiency of ***m*-BBTPI** in solid state is lower than that of **BBTPI** (0.59 versus 0.82). As the two molecules are composed of the same PI emitting units with only small differences in their linking mode, the difference in their photoluminescent efficiency is more likely to be originated from the differences in their overall molecular

conjugation instead of their emitting moieties. It has be pointed out that photoluminescent efficiency of a molecule decreases with the conjugation length given other factors unchanged.[18] Evidently, the conjugation extent of ***m*-BBTPI** is smaller than that of **BBTPI**, which is attributed to the conjugation disruption stemming from ***m*-BBTPI**'s *meta*-architecture,[18a] thus leading to relatively low Φ_{PL} of ***m*-BBTPI**. The optical energy gap (E_g), as determined from the optical absorption threshold, is 3.21 eV. The highest occupied molecular orbital (HOMO) level measured by UPS is -5.34 eV. On other hand, the lowest unoccupied molecular orbital (LUMO) energy, as determined by subtracting the energy gap from the HOMO energy, is -2.13 eV.

Table 1 Summary of the physical data of ***m*-BBTPI** and **BBTPI**.

emitter	T_d^a/T_g^b (°C)	$\lambda_{abs}/\lambda_{em}{}^c$ (nm)	$\lambda_{em}{}^d$ (nm)	Φ^c/Φ^d (%)	E_g/HOMO/LUMO (eV)
***m*-BBTPI**	512/190	263, 334/406	432	70/59	3.21/-5.34/-2.13
BBTPI	481/192	261, 367/427	448	93/82	3.08/-5.56/-2.48

[a] 5% weight loss temperature. [b] Glass transition temperature. [c] Measured in dilute CH_2Cl_2 solution. [d] Measured in film.

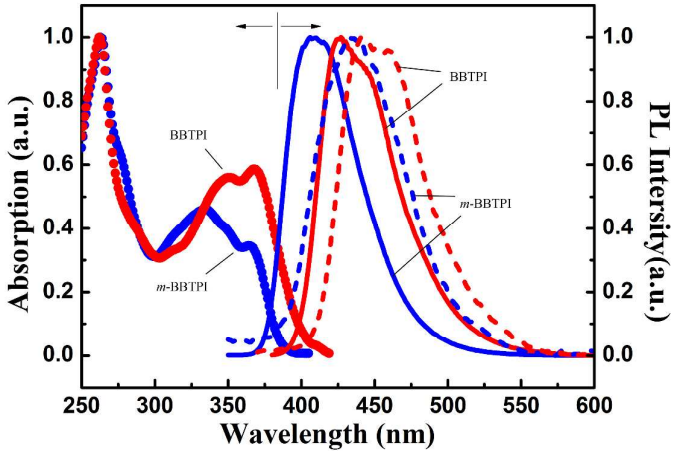

Fig. 2 Absorption and PL spectra of ***m*-BBTPI** and **BBTPI** in dilute CH_2Cl_2 (solid line), and in vacuum-deposited film (dashed line).

3.3 Theoretical calculation

To better understand the correlation between molecular structures and physical properties, theoretical molecular orbital calculations for ***m*-BBTPI** and **BBTPI** were performed with Gaussian 09 at B3LYP/6-31G (d) level. The optimized geometries and calculated frontier molecular orbital electron density distributions are shown schematically in Fig. 3. Both of the two compounds show a similar twisting configuration. Generally, due to the different electrical structures, the steric effect of five-membered rings is intrinsically smaller than that of six-membered counterparts. Therefore, the dihedral angle between imidazole ring and the 2-position linked benzene (around 25°, see Fig. 3) is smaller than that of the two six-membered benzene rings at the center of molecule (~36°). Comparing to BPPI and its isomers (*L*-BPPI and *Z*-BPPI),[16] the additional phenyl in the bridging section of **BBTPI**/***m*-BBTPI** can efficiently limit π conjugation via molecular rotation. Like most PI derivatives,[13a,b] the

side-capping *tert*-butylphenyl groups in ***m*-BBTPI** molecule are high twisted (~78°) with the PI units in the molecules, and have little contribution to frontier orbital electron density distributions. This can play a key role in suppressing emissive redshifts by hindering close molecular packing in solid state, consequently leading to good colour purity as well as stable amorphous thin film.

As shown in Fig. 3, electron density distributions are spatially different in these two molecules, originating from their diverse conjugation linkages. However, the electron cloud distributions of HOMO are mainly located at electron-rich PI moieties,[9d,16] while the LUMO electron clouds are dispersed at the bridging sections. This characteristics of frontier orbital distribution indicate that the PI moieties in the two bisphenanthroimidazole derivatives act as weak electron donors, which is beneficial to hole transporting.

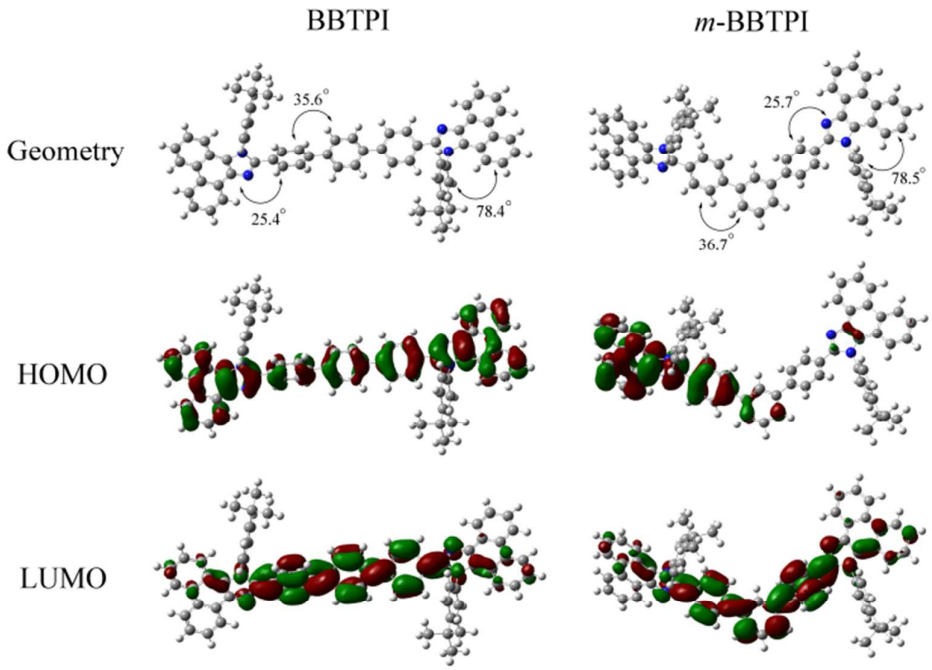

Fig. 3 Optimized geometries, calculated HOMO and LUMO electron density distributions of **BBTPI** and ***m*-BBTPI**.

3.3 Electrical properties

To study the relationship between the molecular structures and charge transporting properties, hole- and electron-only devices were fabricated with respectively configurations of indium tin oxide (ITO)/4,4'-bis[*N*-(1-naphthyl)-*N*-phenylamino]-biphenyl (NPB) (20 nm)/**BBTPI** or ***m*-BBTPI** (50 nm)/NPB (20 nm)/Al (100 nm) and ITO/1,3,5-tris(1-phenyl-1*H*-benzimidazol-2-yl)benzene (TPBI) (20 nm)/**BBTPI** or ***m*-BBTPI** (50 nm)/TPBI (20 nm)/LiF (1 nm)/Al (100 nm). Herein, NPB and TPBI are respectively used for blocking electrons and holes.[19]

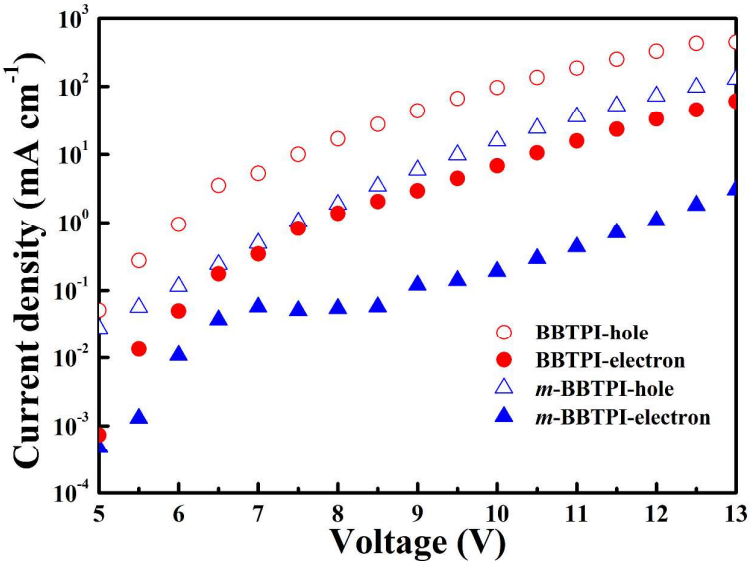

Fig. 4 Electron and hole current densities versus applied voltage of the single carrier devices based on **BBTPI** and ***m*-BBTPI**.

As shown in Fig. 4, the current density-voltage (*J*-*V*) characteristics of the hole- and electron-only devices illustrate that both of the two emitters have bipolar charge transporting capacity as evidenced by the considerable hole/electron current density with similar magnitudes comparing to a complete OLED. Similar to most organic materials,[20] we can find that hole currents are also higher than those of electron in the two bisphenanthroimidazole derivatives. According to the charge-hopping theory of organic solids[21] and analyzing with the theoretical results, this may be due to the dominant contribution of the two peripheral PI groups to HOMO, which benefits the HOMO intermolecular overlaps in solid state. On the other hand, the LUMO electron clouds are mainly located at the central bridging sections. Based on the features of molecular geometries, it is different to achieve efficient intermolecular wave function overlaps in LUMOs, which would lead to relatively low electron transporting properties. It can be seen from Fig. 4 that the charge transporting property of **BBTPI** is superior to that of ***m*-BBTPI**. It can be explained by its symmetrical and linear molecular configuration with relatively ordered and congested solid packing, leading to higher electrical properties.[13e]

3.4 Electroluminescent properties

A non-doped blue-emitting device was fabricated with a configuration of ITO/NPB (70 nm)/4,4',4"-tris(carbazol-9-yl)-triphenylamine (TCTA) (5 nm)/***m*-BBTPI** (30 nm)/TPBI (30 nm)/LiF (1 nm)/Al (150 nm), in which ***m*-BBTPI** was used as non-doped emission layer (EML). Herein, NPB and TPBI served as hole-transporting and electron-transporting materials respectively, while a thin TCTA layer was used to confine excitons within EML.[9a] Fig. S1 presents the device configuration and the energy levels of the used materials. Well-matched energy level alignment was achieved among the contiguous functional layers in as-fabricated device. The key device performances are listed in Table 2. For comparison, the EL properties of **BBTPI** with the same device structure are also presented.

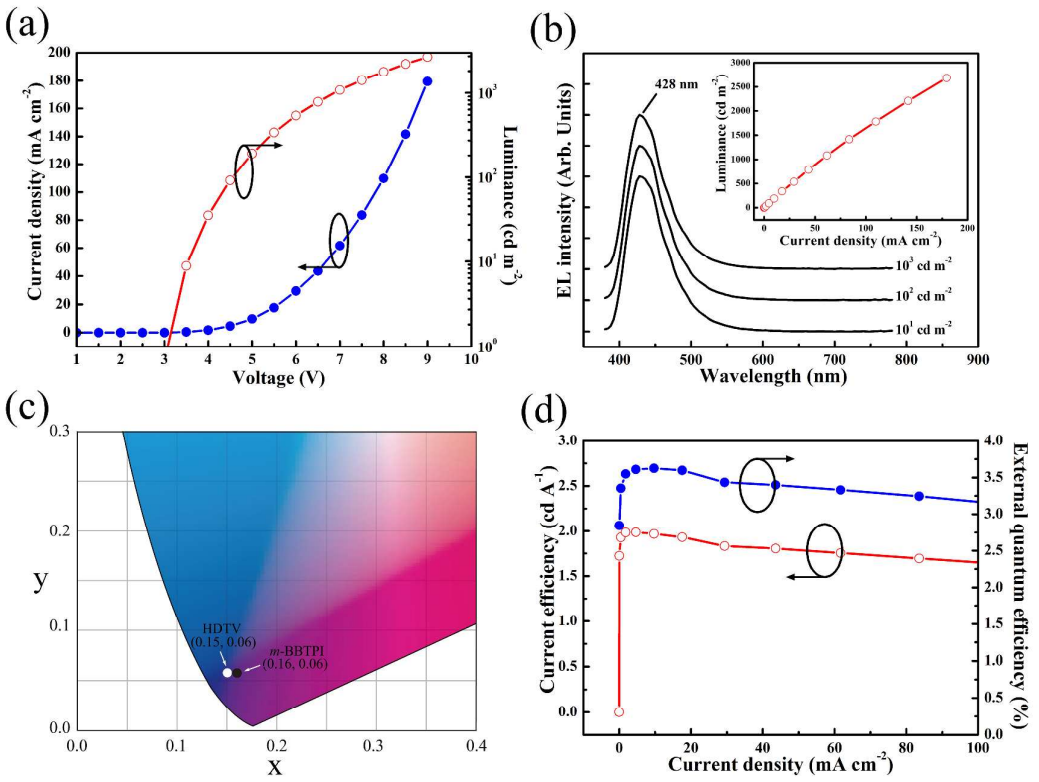

Fig. 5 (a) Current density-voltage-luminescence characteristics, (b) EL spectra at different luminescence and luminescence-current density plot (inset), (c) CIE coordinates and (d) plots of current efficiency and external quantum efficiency versus current density of the ***m*-BBTPI**-based non-doped OLEDs.

Current density-luminance characteristics of the ***m*-BBTPI**-based device are shown in Fig. 5a. A low turn-on voltage (3.2 V, voltage at 1 cd m^{-2}) was obtained. This value is higher than that of the **BBTPI**-based device (2.7 V) and is mainly attributed to ***m*-BBTPI**'s larger E_g (Table 1), giving rise to higher barrier for charge injection. Significantly, the ***m*-BBTPI**-based device emits violet-blue light peaking at 428 nm (Fig. 5b), which shows an evident blueshift compared to that of the **BBTPI**-based device (λ_{em} = 448 nm).[13e] Moreover, EL spectrum of this device shows little change over a wide brightness range from 10 to 1,000 cd m^{-2} (Fig. 5b) and a linear increase of luminescence with respect to current density (inset of Fig. 5b), indicating little current-induced fluorescence quenching in the device. Noticeably, the CIE coordinates of the ***m*-BBTPI**-based device is (0.16, 0.06), which is very close to the standard blue coordinates of High-Definition Television (HDTV) (0.15, 0.06),[22] as shown in Fig. 5c.

Maximum current efficiency (CE) of the ***m*-BBTPI**-based device is 1.99 cd A^{-1} (Fig. 5d). Comparing to the performances of the **BBTPI**-based device (Table 2),[13e] this photometric efficiency appears to be lowered by the molecular tailoring via *meta*-linkage. However, it has to be pointed out that the human eye sensitivity drops dramatically over the short wavelength region,[23] leading to difficulty in achieving high CE in violet-blue OLEDs. For instance, the human eye sensitivity decreases by ~70% from 450 to 430 nm. Therefore, the performance of

the ***m*-BBTPI**-based device is still compared favorably when the sensitivity of human eye is taken into consideration.

On the other hand, the EQE of the **BBTPI**-based device is also higher than that of the ***m*-BBTPI**-based device (3.63% versus 5.77%, Table 2). This can be explained as follows. The EQE of an OLED can describes as,[24]

$$EQE = \gamma\ \Phi_{pl}\ \eta_{oc}\ \eta_{exc} \quad (1);$$

where γ is the recombination efficiency of injected holes and electrons, which is assumed to be 1;[25] Φ_{pl} is the intrinsic PL efficiency; η_{oc} is the optical out-coupling factor; η_{exc} is the exciton utilizing efficiency. It is expected that the values of η_{exc} are similar in the **BBTPI**- and the ***m*-BBTPI**-based devices with similar molecular structure for the emitter and the same device architecture. As we discussed, **BBTPI** has a linear planar molecular geometry.[13e] Thus, it is expected that the η_{oc} of the **BBTPI**-based device is larger than the ***m*-BBTPI**-based device. Meanwhile, the Φ_{pl} of ***m*-BBTPI** is smaller than that of **BBTPI** due to the conjugation decrease. Therefore, the EQE the **BBTPI**-based device is superior to the ***m*-BBTPI**-based device.

Table 2 Summary of the device performances of the ***m*-BBTPI**- and the **BBTPI**-based non-doped OLEDs.

emitter	V_{on} (V)	λ_{EL} (nm)	CE[a] (cd A^{-1})	PE[b] (lm W^{-1})	EQE[c] (%)	CIE (x, y)
***m*-BBTPI**	3.2	428	1.99, 1.97, 1.77	1.81, 1.42, 0.82	3.63, 3.61, 3.36	0.16, 0.06
BBTPI	2.7	448	5.48, 5.35, 5.10	4.77, 4.41, 2.90	5.77, 5.60, 5.41	0.15, 0.10

[a] Current efficiency, [b] power efficiency, [c] external quantum efficiency corresponding to the value at the maximum, 100 cd m^{-2} and 1000 cd m^{-2}, respectively.

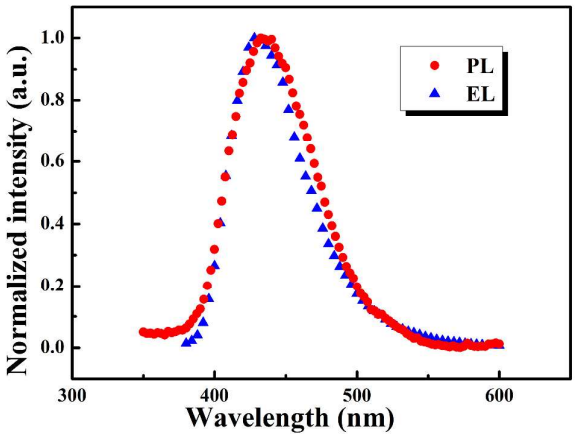

Fig. 6 Comparison between the PL spectrum of ***m*-BBTPI** in solid state and the EL spectrum of the ***m*-BBTPI**-based device.

Although performance of the violet-blue ***m*-BBTPI**-based device is lower than its blue counterpart, it is markedly improved in comparison with those of *L*-BPPI- and *Z*-BPPI-based devices.[16] Analyzing the device structures carefully, the TCTA layer also plays a key role in achieving higher efficiency in this work. In fact, the bisphenanthroimidazole derivatives are high-energy-gap compounds, with E_g larger than 3.00 eV (3.21, 3.15, 3.30 eV for ***m*-BBTPI**,

L-BPPI and *Z*-BPPI respectively). In the device structures of this work and previous work by Wang *et al.*,[16] NPB (E_g = ~3.00 eV) layer was used as hole-transporting layer (HTL). Provided that NBP HTL was deposited in proximity to bisphenanthroimidazole derivatives-based EML, the excitons generated by the recombination of the injected carriers in the EML would leak into HTL due to the relatively small E_g of NPB. This can be supported by the evidence that EL emissions of the *L*-BPPI- and *Z*-BPPI-based devices mismatch their corresponding intrinsic PL emissions. In this work, we applied a TCTA (E_g = ~3.40 eV) layer as buffer layer,[9a] so as to confine the excitons within the EML. As shown in Fig. 6, the EL spectrum of ***m*-BBTPI**-based device is similar to the PL emission of ***m*-BBTPI**, implying efficient confinement of excitons. To obtain a comprehensive comparison, key device performance parameters of ***m*-BBTPI** and recently reported non-doped violet-blue OLEDs are listed in Table S1.[6b,9b-e,13e] It can be seen that the device performances of the ***m*-BBTPI**-based device are comparable to the highly efficient non-doped violet-blue OLEDs. All the above evidences indicate that the strategies used in this work for violet-blue OLEDs is effective.

Conclusions

In summary, a novel violet-blue fluorophor ***m*-BBTPI** has been designed with the strategy jointing two TPI units using a freely rotatable benzene ring via the *meta*-linkage. In this work, the relationships between modification in molecular structure and various materials' properties, including thermal stabilities, photophysical characteristics, theoretical frontier orbital distributions as well as charge transporting properties, are comprehensively discussed. We find that the new compound ***m*-BBTPI** exhibits good thermal stability, efficient violet-blue emission and bipolar charge transporting characteristics. Finally, the differences of device performances originating from chemical structure adjustment for emitter are analyzed. By using a suitable device structure, OLED based on ***m*-BBTPI** as a non-doped EML exhibits decent performance with CE (PE) up to 1.99 cd A^{-1} (1.81 lm W^{-1}) and a colour index of (0.16, 0.06), which is comparable to the reported efficient non-doped violet-blue devices.

Acknowledgements

This research was supported by the Research Grants Council of the Hong Kong (Project No. T23-713/11), the National Natural Science Foundation of China (Project Nos. 51273108 and 91027041) and the National Basic Research Program of China (973 Program No. 2013CB834803).

References

1 Z. Hao, J. Zhang, X. Zhang, X. Ren, Y. Luo and S. Lu, *J. Phys. D: Appl. Phys.*, 2008, **41**, 182001.

2 D. S. Thakare, S. K. Omanwar, P. L. Muthal, S. M. Dhopte, V. K. Kondawar and S. V. Moharil, *Phys. Status Solidi (a)*, 2004, **201**, 574-581.

3 L. T. T. Nhung, H. Nagata, A. Takahashi, M. Aihara, T. Okamoto, T. Shimohata, K. Mawatari, M. Akutagawa, Y. Kinouchi and M. Haraguchi, *J. Med. Invest.*, 2012, **59**, 53-58.

4 T.-W. Kuo, C.-H. Huang and T.-M. Chen, *Appl. Opt.*, 2010, **49**, 4202-4206.

5 (a) J. Kido, H. Shionoya and K. Nagai, *Appl. Phys. Lett.*, 1995, **67**, 2281-2283; (b) J.-H. Jou, Y.-S. Chiu, R.-Y. Wang, H.-C. Hu, C.-P. Wang and H.-W. Lin, *Org. Electron.*, 2006, **7**, 8-15; (c) C. H. Chuen, Y. T. Tao, F. I. Wu and C. F. Shu, *Appl. Phys. Lett.*, 2004, **85**, 4609-4611.

6 (a) P. I. Shih, C. Y. Chuang, C. H. Chien, E. W. G. Diau and C. F. Shu, *Adv. Funct. Mater.*, 2007, **17**, 3141-3146; (b) Z. Gao, Y. Liu, Z. Wang, F. Shen, H. Liu, G. Sun, L. Yao, Y. Lv, P. Lu and Y. Ma, *Chem. Eur. J.*, 2013, **19**, 2602-2605; (c) S. J. Lee, J. S. Park, K.-J. Yoon, Y.-I. Kim, S.-H. Jin, S. K. Kang, Y.-S. Gal, S. Kang, J. Y. Lee, J.-W. Kang, S.-H. Lee, H.-D. Park and J.-J. Kim, *Adv. Funct. Mater.*, 2008, **18**, 3922-3930.

7 (a) J. H. Wilkens and R. Stirne, U.S. 6902563, 2005; (b) C. Bolta, U.S. 7015636, 2006.

8 (a) Y. Li and L. Jin, *Environ. Eng. Sci.*, 2011, **28**, 687-691; (b) D. D. Shao, S. C. Wu, P. Liang, Y. Kang, W. J. Fu, K. L. Zhao, Z. H. Cao and M. H. Wong, *J. Hazard. Mater.*, 2012, **221-222**, 28-34.

9 (a) C. C. Wu, Y. T. Lin, K. T. Wong, R. T. Chen and Y. Y. Chien, *Adv. Mater.*, 2004, **16**, 61-65; (b) S. Tang, M. Liu, P. Lu, H. Xia, M. Li, Z. Xie, F. Shen, C. Gu, H. Wang, B. Yang and Y. Ma, *Adv. Funct. Mater.*, 2007, **17**, 2869-2877; (c) J. Ye, Z. Chen, M.-K. Fung, C. Zheng, X. Ou, X. Zhang, Y. Yuan and C.-S. Lee, *Chem. Mater.*, 2013, **25**, 2630-2637; (d) Y. Yuan, J.-X. Chen, F. Lu, Q.-X. Tong, Q.-D. Yang, H.-W. Mo, T.-W. Ng, F.-L. Wong, Z.-Q. Guo, J. Ye, Z. Chen, X.-H. Zhang and C.-S. Lee, *Chem. Mater.*, 2013, **25**, 4957-4965; (e) Z. Gao, G. Cheng, F. Shen, S. Zhang, Y. Zhang, P. Lu and Y. Ma, *Laser Photonics Rev.*, 2014, **8**, L6-L10.

10 (a) J. Huang, N. Sun, Y. Dong, R. Tang, P. Lu, P. Cai, Q. Li, D. Ma, J. Qin and Z. Li, *Adv. Funct. Mater.*, 2013, **23**, 2329-2337; (b) C. H. Chien, C. K. Chen, F. M. Hsu, C. F. Shu, P. T. Chou and C. H. Lai, *Adv. Funct. Mater.*, 2009, **19**, 560-566; (c) C. J. Tonzola, A. P. Kulkarni, A. P. Gifford, W. Kaminsky and S. A. Jenekhe, *Adv. Funct. Mater.*, 2007, **17**, 863-874.

11 S. H. Kim, I. Cho, M. K Sim, S. Park and S. Y. Park, *J. Mater. Chem.*, 2011, **21**, 9139-9148.

12 (a) A. P. Kulkarni, C. J. Tonzola, A. Babel and S. A. Jenekhe, *Chem. Mater.*, 2004, **16**, 4556-4573; (b) Y. Shirota and H. Kageyama, *Chem. Rev.*, 2007, **107**, 953-1010.

13 (a) Y. Zhang, S.-L. Lai, Q.-X. Tong, M.-F. Lo, T.-W. Ng, M.-Y. Chan, Z.-C. Wen, J. He, K.-S. Jeff, X.-L. Tang, W.-M. Liu, C.-C. Ko, P.-F. Wang and C.-S. Lee, *Chem. Mater.*, 2012, **24**, 61-70; (b) Y. Zhang, S.-L. Lai, Q.-X. Tong, M.-Y. Chan, T.-W. Ng, Z.-C. Wen, G.-Q. Zhang, S.-T. Lee, H.-L. Kwong and C.-S. Lee, *J. Mater. Chem.*, 2011, **21**, 8206-8214; (c) W. Li, D. Liu, F. Shen, D. Ma, Z. Wang, T. Feng, Y. Xu, B. Yang and Y. Ma, *Adv. Funct. Mater.*, 2012, **22**, 2797-2803; (d) Y. Yuan, D. Li, X. Q. Zhang, X. J. Zhao, Y. Liu, J. Y. Zhang and Y. Wang, *New J. Chem.*, 2011, **35**, 1534-1540; (e) W.-C. Chen, Y. Yuan, G.-F. Wu, H.-X. Wei, L. Tang, Q.-X. Tong, F.-L. Wong and C.-S. Lee, *Adv. Optical Mater.*, 2014, **2**, 626-631; (f) W.-C. Chen, Y. Yuan, G.-F. Wu, H.-X. Wei, J. Ye, M. Chen, F. Lu, Q.-X. Tong, F.-L. Wong and C.-S. Lee, *Org. Electron.*, 2015, **17**, 159-166; (g) Y. Yuan, J.-X. Chen, W.-C. Chen, S.-F. Ni, H.-X. Wei, J. Ye, F.-L. Wong, Z.-W. Zhou, Q.-X. Tong and C.-S. Lee, *Org. Electron.*, 2015, **18**, 61-69; (h) K. Wang, S. Wang, J. Wei, Y. Miao, Y. Liu and Y. Wang, *Org. Electron.*, 2014, **15**, 3211-3220; (i) K.

Wang, S. Wang, J. Wei, S. Chen, D. Liu, Y. Liu and Y. Wang, *J. Mater. Chem. C*, 2014, **2**, 6817-6826; (j) Z. Gao, Z. Wang, T. Shan, Y. Liu, F. Shen, Y. Pan, H. Zhang, X. He, P. Lu, B. Yang and Y. Ma, *Org. Electron.*, 2014, **15**, 2667-2676. (k) H. Huang, Y. Wang, S. Zhuang, X. Yang, L. Wang and C. Yang, *J. Phys. Chem. C*, 2012, **116**, 19458-19466; (l) X. Zhang, J. Lin, X. Ouyang, Y. Liu, X. Liu and Z. Ge, *J. Photochem. Photobiol. A*, 2013, **628**, 37-43; (m) H. Huang, Y. Wang, B. Wang, S. Zhuang, B. Pan, X. Yang, L. Wang and C. Yang, *J. Mater. Chem. C*, 2013, **1**, 5899-5908.

14 (a) A. Richaud, N. Barba-Behrens and F. Méndez, *Org. Lett*., 2011, **13**, 972-975; (b) Z. Wang, Y. Feng, S. Zhang, Y. Gao, Z. Gao, Y. Chen, X. Zhang, P. Lu, B. Yang, P. Chen, Y. Ma and S. Liu, *Phys. Chem. Chem. Phys.*, 2014, **16**, 20772-20779.

15 Z. M. Wang, P. Lu, S. M. Chen, Z. Gao, F. Z. Shen, W. S. Zhang, Y. X. Xu, H. S. Kwok and Y. G. Ma, *J. Mater. Chem.*, 2011, **21**, 5451-5456.

16 Z. Wang, Y. Feng, H. Li, Z. Gao, X. Zhang, P. Lu, P. Chen, Y. Ma and S. Liu, *Phys. Chem. Chem. Phys.*, 2014, **16**, 10837-10843.

17 N. Miyaura and A. Suzuki, *Chem. Rev.*, 1995, **95**, 2457-2483.

18 (a) J.-X. Qiu, Y.-X. Li, X.-F. Yang, Y. Nie, Z.-W. Zhang, Z.-H. Chen and G.-X. Sun, *J. Mater. Chem. C*, 2014, **2**, 5954-5962; (b) Y. Yamaguchi, Y. Matsubara, T. Ochi, T. Wakamiya and Z.-i. Yoshida, *J. Am. Chem. Soc.*, 2008, **130**, 13867-13869.

19 (a) W. Jiang, L. Duan, J. Qiao, G. Dong, L. Wang and Y. Qiu, *Org. Lett.*, 2011, **13**, 3146-3149; (b) K. Wang, F. S. Zhao, C. G. Wang, S. Y. Chen, D. Chen, H. Y. Zhang, Y. Liu, D. G. Ma and Y. Wang, *Adv. Funct. Mater.*, 2013, **23**, 2672-2680.

20 L. S. Hung and C. H. Chen, *Mater. Sci. Eng. R*, 2002, **39**, 143-222.

21 W. Brutting, ed., *Physics of organic semiconductors*, Wiley-VCH, New York, 2005.

22 T. Tsujimura, *OLED display fundamentals and applications*, Wiley, 2012.

23 (a) E. F. Schubert and J. K. Kim, *Science* 2005, **308**, 1274-1278; (b) S. R. Forrest, D. D. C. Bradley and M. E. Thompson, *Adv. Mater.*, 2003, **15**, 1043-1048.

24 Q. Wang and D. Ma, *Chem. Soc. Rev.*, 2010, **39**, 2387-2398.

25 S. T. Zhang, W. J. Li, L. Yao, Y. Y. Pan, F. Z. Shen, R. Xiao, B. Yang and Y. G. Ma, *Chem. Commun.*, 2013, **49**, 11302-11304.

Graphical Abstract

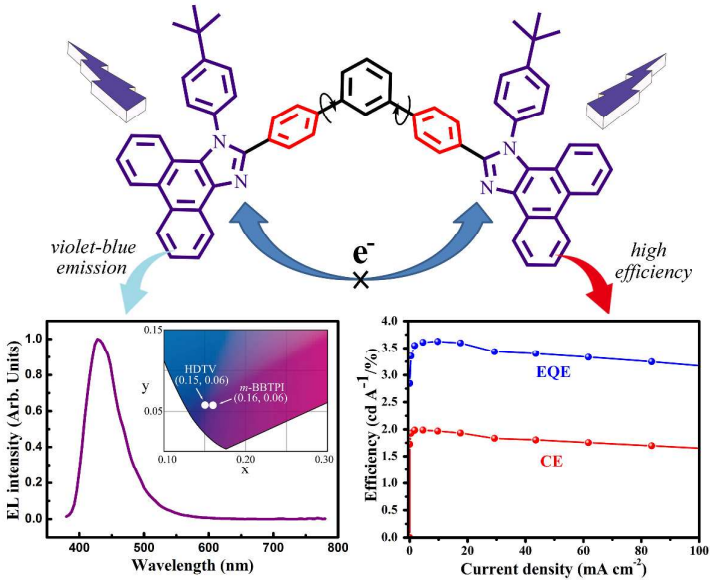

In this study, a novel violet-blue emitter *m*-BBTPI was designed and synthesized via *meta*-molecular tailoring. Using *m*-BBTPI as non-doped emitter, we obtained a high-efficiency violet-blue organic electroluminescent device.